Review

Electron Paramagnetic Resonance Spin Trapping (EPR–ST) Technique in Photopolymerization Processes

Fabienne Peyrot [1,2,*] 🔲, Sonia Lajnef [1] and Davy-Louis Versace [3,*]

1 Laboratoire de Chimie et Biochimie Pharmacologiques et Toxicologiques, Université Paris Cité, 75006 Paris, France
2 Institut National Supérieur du Professorat et de l'Éducation (INSPE) de l'Académie de Paris, Sorbonne Université, 10 rue Molitor, 75016 Paris, France
3 Institut de Chimie et des Matériaux Paris-Est (ICMPE, UMR CNRS 7182), Université Paris-Est Créteil (UPEC), 2-8 rue Henri Dunant, 94320 Thiais, France
* Correspondence: fabienne.peyrot@u-paris.fr (F.P.); davy-louis.versace@u-pec.fr (D.-L.V.)

Abstract: To face economic issues of the last ten years, free-radical photopolymerization (FRP) has known an impressive enlightenment. Multiple performing photoinitiating systems have been designed to perform photopolymerizations in the visible or near infrared (NIR) range. To fully understand the photochemical mechanisms involved upon light activation and characterize the nature of radicals implied in FRP, electron paramagnetic resonance coupled to the spin trapping (EPR–ST) method represents one of the most valuable techniques. In this context, the principle of EPR–ST and its uses in free-radical photopolymerization are entirely described.

1. Introduction

In recent decades, photopolymerization has gained an incredible growing interest and has been employed in many common applications [1–5] in coatings, microelectronics, medicine, inks, dentistry, and 3D-printing technology. Photochemical processes have also been put forward by valuable applications [6–14] in surface functionalization, biomaterial synthesis, photoactivable materials, visible light-induced controlled polymerizations, two-photon polymerization, and so forth. Contrary to thermal-induced polymerization, light-induced polymerization demonstrates some striking advantages [1,3] such as low energy consumption without the use of solvents, mild experimental conditions, and few side reactions. Additionally, photopolymerization promotes fast reactions in a few seconds versus hours with the thermal process, thus making photopolymerization an environmentally friendly process. To date, two different photochemical mechanisms [1] (cationic and free-radical photopolymerizations; CP and FRP, respectively) have dominated most of the academic and industrial studies. Particularly, FRP is a widely performed technique to design polymer materials [15]. FRP has been extensively used, and many specialized reviews [15–17] have been already published. In this process, polymerization occurs using two types of photo-initiators which differ in the way that radical species are formed under light irradiation [3]. Type I photo-initiators are aromatic carbonyl organic molecules that undergo a "α-cleavage" to generate free-radical species, contrary to Type II-initiating systems, which are usually implying electron/proton transfer reactions when combined with co-initiators (thiols, tertiary amines, or alcohols, for instance). Recently, a huge number of performing photo-initiating systems has been synthesized to perform FRP in the UV–visible and NIR ranges [18–24]. In order to design the most efficient photo-initiators/photocatalysts, and to fully understand the photochemical mechanisms involved upon light activation, electron paramagnetic resonance (EPR, equivalent to ESR, electron spin resonance) represents one of the most valuable techniques. In association with spin

trapping, EPR now appears as an invaluable method to detect and characterize all kinds of radicals produced by photo-initiating systems (PIS) under light excitation. In this review, we will describe the principle of EPR–ST and give an overview of its application to free-radical polymerization, with a special attention to technological and methodological requirements.

2. Spin Trapping Principle and Brief Description of EPR Spectra

Most radicals formed following PIS irradiation are highly reactive and short-lived. Their steady-state concentration rarely reaches measurable levels by direct observation, with conventional X-band spectrometers operating at ≈ 9.8 GHz. The use of spin traps allows this limitation to be overcome through radical stabilization and indirect detection. In a spin trapping experiment, a reactive radical performs an addition reaction to a diamagnetic molecule, the spin trap, yielding a more stable radical product called the spin adduct, which accumulates to concentrations above the detection threshold (Figure 1). The first spin trapping experiments by Iwamura and Inamoto with the cyclic nitrone DMPO (5,5-dimethyl-1-pyrrolidine N-oxide; Figure 1) in chemical systems date back to 1967 [25], and the method was further developed by Janzen and Blackburn [26], who coined the terms spin trap and spin trapping. Applications in all the fields of in-solution chemistry, which involve radical intermediates, have since been proposed, and very intense research in spin trap synthesis has considerably extended the panel of spin trapping agents [27–29]. Lalevée et al. generalized its use in the field of PIS studies [30].
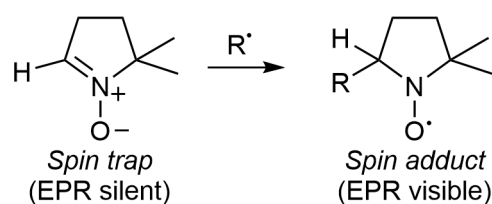

Figure 1. Principle of spin trapping with DMPO. The short-lived radical R[•] adds to the cyclic nitrone to form a persistent nitroxide radical that can be detected by EPR.

Spin traps are generally not selective of one radical, but the spin adduct displays a distinctive EPR spectrum that gives information about the trapped radical species. A typical spectrum of an aminoxyl (nitroxide) spin adduct derived from DMPO is presented in Figure 2. The g-value is calculated from B_0, the magnetic field at the centre of the spectrum, and ν, the working frequency of the spectrometer, using the equation $g = h\nu/(\beta B_0)$ (where h is the Planck constant and β the Bohr magneton). The parameter g is generally between 2.005 and 2.007 for all nitroxides and varies only slightly with the structure of the radical. The splitting of EPR lines in the spectra originates from the so-called hyperfine interaction of the unpaired electron spin with the non-zero nuclear spin I of neighbouring atoms (each interaction splits the signal into $2nI + 1$ lines, with n being the number of interacting nuclei). In the present example in Figure 2, two hyperfine splittings (HFS), a_N and a_H, can be read from the spectrum arising from the interaction with nitrogen-14 (I = 1, > 99.6% of natural nitrogen) and with the proton in the β-position to the nitrogen (I = 1/2), respectively. HFS are expressed in Gauss (G) or millitesla (mT, 1 mT = 10 G). These constants are much more sensitive to the structure of the spin adduct than the g-value. The a_H value is directly related to the dihedral angle between the p orbital of the aminoxyl function and the C–H bond. It thus depends on the nitroxide conformation and is highly influenced by the size of the substituent corresponding to the trapped radical, which hinders the rotation of all groups attached to the aminoxyl function, including the β-hydrogen, but also by the cyclic versus linear character of the spin trap [31]. The ^{14}N interaction is controlled by electron-donating or -withdrawing effects and reports more on the nature of the captured radical. Identification can, however, remain ambiguous, as radicals belonging to the same type may yield very similar or even identical spectra. The ^{14}N coupling constant also increases with the polarity of the solvent used, while the a_H value usually (but not always) decreases [32]. These observations can be partially rationalized by considering the equilibrium between

the two limit mesomeric forms of a nitroxide, since the form displaying a single electron on the nitrogen predominates in polar media (Figure 3). As a consequence, the number of lines for the same radical adduct can change when two HFS become equal by switching the solvent from chloroform to acetonitrile [33], for instance. Thus, researchers should always state the nature of the solvent used in spin trapping experiments.
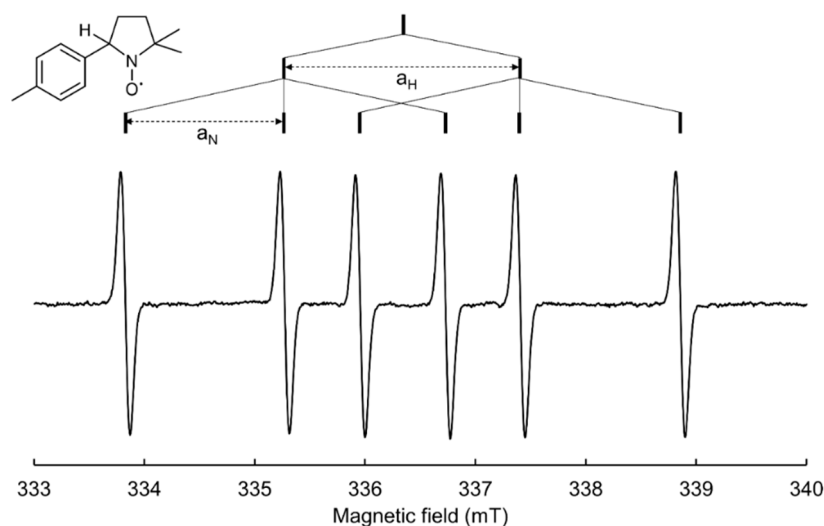

Figure 2. Representative X-band EPR spectrum of the 4-methylphenyl radical spin adduct of DMPO, the structure of which appears in the upper left corner. The stick diagram shown above the spectrum facilitates the interpretation of the hyperfine splitting pattern.

Figure 3. Equilibrium between limit mesomeric forms of a nitroxide.

Several spin traps can be used to obtain complementary information on a PIS photolysis. The most common are either nitroso compounds or nitrones, which can be linear or cyclic. All of them lead to the formation of nitroxide radicals.

3. Three Classes of Spin Traps

3.1. Nitroso Spin Traps

Among nitroso compounds, 1-methyl-1-nitrosopropane (MNP) has been most frequently used in the literature. However, it decomposes upon exposure to light, producing tert-butyl radical, the MNP adducts of which are highly stable and prevent the detection of any other radical species [32]. Nitrosoarene compounds, such as nitrosodurene (ND, i.e., 1,2,4,5-tetramethyl-3-nitrosobenzene, Figure 4), have been preferably applied in the field of photopolymerization studies because of their increased stability towards photolysis [34]. ND is readily soluble in chloroform and dichloromethane and slightly soluble in aromatic hydrocarbons and alcohols. The main advantage of the nitroso spin trap family is the fact that the trapped radical is directly attached to the nitrogen in the spin adduct. Hyperfine couplings arising from the non-zero spins in the radical fragment can therefore report on the identity of the trapped species. For example, the spectra of the (4-methyl)phenyl radical spin adduct of ND, produced upon photoexcitation at 400 nm of allylated purpurin [35] or quinizarine [23] in the presence of a iodonium salt in benzene, display hyperfine couplings with every proton present in the 4-methylphenyl fragment ($a_N = 10.27$ G, $a_{Hmeta,1} = 0.93$ G, $a_{Hmeta,2} = 0.93$ G, $a_{Hortho,1} = 2.87$ G, $a_{Hortho,2} = 2.70$ G,

$a_{H(CH3)para,1}$ = 3.08 G, $a_{H(CH3)para,2}$ = 3.08 G, and $a_{H(CH3)para,1}$ = 3.05 G) (Figure 5). Interestingly, the absence of resolved proton hyperfine couplings arising from the 2,3,5,6-tetramethylphenyl system suggests that spin delocalization into this ring is small, and that the aminoxyl group is twisted away from the corresponding plane.

(a) Spin trapping with ND
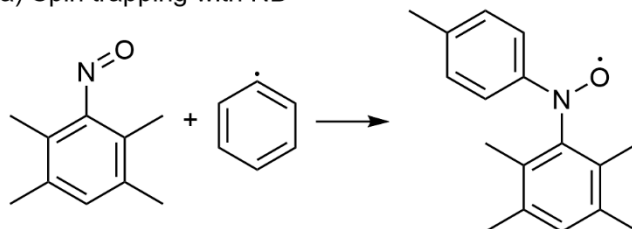
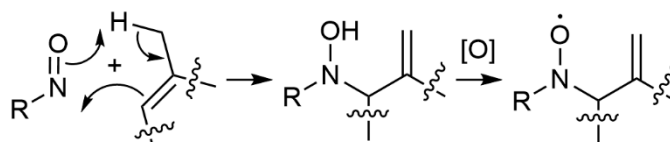(b) Ene-reaction with nitroso spin trap and alkenes

Figure 4. Typical reactions of nitroso spin traps: (**a**) spin trapping reaction of 4-methylphenyl radical by ND; (**b**) undesired ene-reaction with an alkene; the hydroxylamine formed in the pericyclic reaction is rapidly converted to a nitroxide in the presence of oxygen or another oxidant.
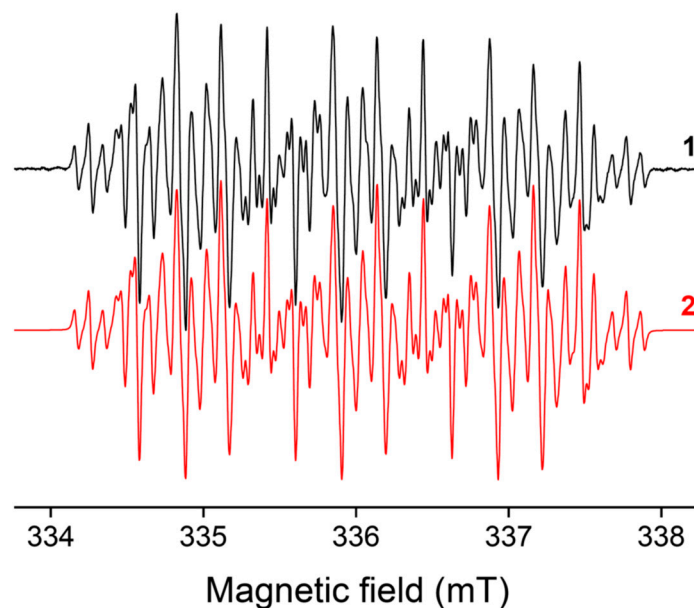
Figure 5. The experimental (1) and simulated (2) EPR spectra of the 4-methylphenyl radical spin adduct of ND produced upon photoexcitation of allylated purpurin and an iodonium salt in benzene. Reproduced from Ref. [35]. Copyright 2021 permission Royal Society of Chemistry.

ND is suitable for the detection of phosphorus-centred radicals [36], such as the diphenylphosphinyl radical Ph$_2$P$^\bullet$, but has not been applied for this purpose in the field of PIS studies to our knowledge.

Yet, the use of nitroso spin traps is limited due to several disadvantages. Nitroso compounds are generally in equilibrium with their dimers in solution, which do not perform spin trapping reactions. Formation of nitroxides following the unwanted ene-reaction between the spin trap and carbon–carbon double bonds may also seriously interfere with the detection when alkenes [32] are present (Figure 4). Silyl radical adducts of nitroso

compounds [37] are also unstable at room temperature and are scarcely detected. Finally, the high toxicity of nitroso spin traps limits their use in photochemical applications.

3.2. Linear Nitrone Spin Traps

The parent compound for all linear nitrone spin traps and widely used in the field of PIS studies is *N-tert-α*-phenyl-butylnitrone (PBN) (Figure 6). It is a commercially available solid, appropriate for use in all media and an especially good trap for carbon-based radical, while the spin adducts derived from oxygen-centred radicals may prove unstable. In the case of nitrone spin traps, both linear and cyclic, the $R^\bullet$ radical adds onto the carbon of the nitrone function and not directly to the nitrogen. Consequently, the nuclei with non-zero spin in the R group are often too far to produce resolved hyperfine coupling. Most spectra are characterized by only six lines arising from the coupling with the nitrogen and hydrogen in the β position. The a_N values of PBN spin adducts of carbon centred radicals (14.3–14.9 G) are larger than those of oxygen-centred radicals (13.3–14.2 G) due to the reduced electronegative character of the captured radical. This range of variation being rather small, precise identification of the trapped radical with PBN is not always possible. A β-phosphorylated derivative, PPN (i.e., diethyl 1-(*N*-benzylidene *N*-oxyamino) 1-methylethyl phosphonate), has been proposed (Figure 6), which facilitates the identification of the trapped species [38] thanks to a large and structure-sensitive additional ^{31}P hyperfine coupling constant (I = ½ , 100% natural abundance). The latter being not commercially available, it has not been used for PIS studies yet despite its ability to trap both carbon-and oxygen-based radicals. PBN is the most commonly used spin-trap in photopolymerization investigations, and the detection of radical species (i.e., acyl, phenyl, phosphinoyl, benzyl, sulfonyl, silyl, germyl, and boryl radicals) generated from PIS has been then systematically generalized by photochemistry groups [30,35,39–42] and described as follows.
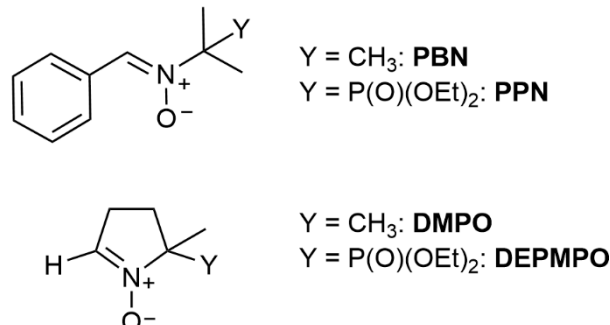

Y = CH$_3$: **PBN**
Y = P(O)(OEt)$_2$: **PPN**

Y = CH$_3$: **DMPO**
Y = P(O)(OEt)$_2$: **DEPMPO**

Figure 6. Selected nitrone spin traps.

3.2.1. Carbon-Centred Radical Spin Adducts of PBN

Initial studies with PBN in the field of PIS studies aimed at detecting the benzoyl radical formed in the course of photolysis of 2,2′-dimethoxyphenyl acetophenone (DMPA), 2-hydroxymethyl-1-phenylpropan-1-one, or benzoin ether derivatives [43–46]. These common photo-initiators (Figure 7) are easily photobleached through a well-known Norrish I cleavage process to form different carbon-centred radical species, as described in Equation (1).

$$\text{Ph-C(O)-R} \rightarrow \text{Ph-C(O)}^\bullet + R^\bullet \tag{1}$$

However, a weak variation of a_N and a_H reflects the change in the benzoyl substituent in PBN spin adducts, where the a_H values range from 4.45 to 4.55 G. Notably, the HFS for the different benzoyl radicals trapped by DMPO increases, and a_H is comprised between 13.97 and 14.41 G. Surprisingly, the dimethoxybenzyl radical is not trapped due to its stabilized character, and PBN seems to be selective towards the other carbon-centred radicals, which are not detected.
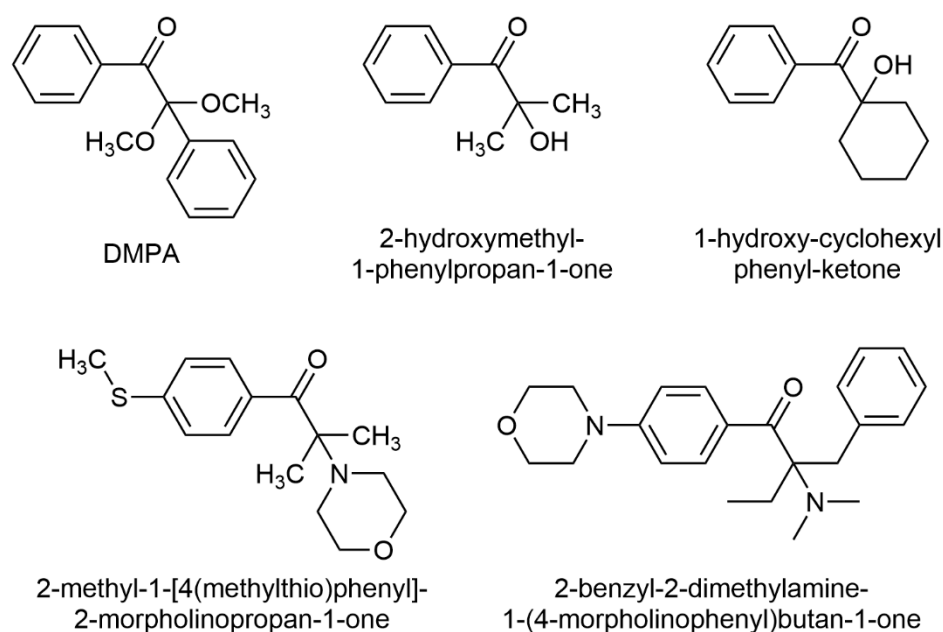
Figure 7. Common type I photo-initiators.

Some other pathways are described in the literature to initiate FRP for the use of amino alkyl or phenyl radicals, which are highly reactive towards acrylate double bonds [3]. The amino alkyl radicals result in a reaction between the triplet excited state of a photosensitizer (benzophenone (BP) or camphorquinone (CQ) for example) and *N*-methyl diethanol amine (MDEA, an electron donor molecule) through an electron transfer followed by an H abstraction reaction process. Although this reaction is now well-established, such radicals have not been trapped by PBN under these conditions. On the contrary, the highly reactive phenyl radicals are mostly generated from the direct photolysis or the photosensibilization of diaryl iodonium (or triarylsulfonium) salts, resulting in a homolytic cleavage of the C–I (C–S) bond. Many examples of investigations implying aryl radical adducts using PBN have been proposed so far. For example, Versace et al. designed new purpurin-based photoinitiating systems [35] in combination with *bis*(4-methylphenyl) iodonium hexafluorophosphate (Iod) as an oxidizing agent. The EPR–ST technique was applied to monitor the formation of (4-methyl)phenyl radicals using PBN, therefore highlighting an electron transfer reaction process between purpurin derivatives and Iod. The (4-methyl)phenyl spin adducts of PBN were described as the main observable components. The EPR signal of the (4-methyl)phenyl adduct is characterized by the following spin-Hamiltonian parameters in benzene: $a_N = 14.52$ G and $a_H = 2.21$ G (g = 2.0061). Interestingly, the generation of phenyl radicals ($a_N = 14.4$ G, $a_H = 2.2$ G) was also observed after the photolysis of triarylsulfonium salts (triarylsulfonium hexafluoroantimonate salts) under UV-light irradiation by EPR–ST [47]. Under mild conditions, phenyl radicals can abstract hydrogen from a polymer backbone allowing thus the UV-induced grafting of polymers on the polymer surface. This new photoinduced process gave the opportunity to tune the functionality of the polymer surface and consequently to control its wettability as a function of the irradiation time. Additionally, Versace et al. used a titanium (iso)propoxide/iodonium salt as an alternative photoinitiating system to synthesize visible-light absorbing Ti-based nanoparticles (NPs) in cationic photopolymerizable films [48]. EPR spin trapping with PBN evidenced the formation of phenyl radicals ($a_N = 14.1$ G and $a_H = 2.1$ G in tert-butylbenzene) and the corresponding peroxyl radicals (PhOO•, $a_N = 13.6$ G and $a_H = 1.6$ G) under air. Multiple additions of peroxyl radicals to Ti• and the multiple fragmentations of the titanium peroxide complexes under UV light irradiation likely occur to form Ti-based NPs.

Recently, new ferrocene-based photoredox catalysts [49] coupled with iodonium salt (di-*tert*-butyl-diphenyl iodonium hexafluorophosphate) have been proposed to generate

aryl radicals (Ar$^\bullet$) used to efficiently initiate FRP. This photoredox reaction leads to an Ar$^\bullet$/PBN radical adduct with HFS of a_N = 14.1 G and a_H = 2.1 G in toluene. Remarkably, the nature of the electron donor group on aryl radicals slightly influences the HFS with PBN. More recently, (9,10-dioxo-9,10-dihydroanthracen-1-yl)(p-tolyl)iodonium trifluoromethane-sulfonate and (4-methoxyphenyl)(4-oxo-2-phenyl-4H-benzo[h]chromen-3-yl)iodonium-4-methylbenzenesulfonate, two new iodonium-based dyes used as a type I photo-initiating systems [21], revealed remarkable initiating properties for FRP thanks to the formation of aryl radicals, which were observed by EPR–ST with HFS constants of a_N = 14.3 G and a_H = 2.2 G in *tert*-butylbenzene.

Among all the type I photo-initiators, the non-common acyloximes are recognized as photo-based generators but are not widely used in FRP. The primary process is a fast N–O cleavage followed by a fast release of carbon dioxide and amino and carbon-centred radicals [50,51]. For example, Chandra et al. [51] designed a new visible absorbing acyloxime used in FRP. According to EPR–ST, only one PBN spin adduct corresponding to benzyl radicals in toluene was observed upon light activation (a_N = 14.3 G and a_H = 2.45 G).

Additionally, EPR–ST was used for the first time to observe the Co(acac)$_2$-mediated radical polymerization of n-butyl acrylate [52]. The C–Co bond photolysis led to the release of alkyl radicals, the formation of which was followed by EPR–ST spectroscopy with PBN in *tert*-butylbenzene. Under these conditions, a specific EPR signal of spin adducts derived from carbon-centred radicals on the polymer backbone with a_N = 14.53 G and a_H = 2.91 G was evidenced, thus confirming the C–Co bond photolysis and the photomediated radical polymerization.

3.2.2. Silyl Radical Spin Adducts of PBN

Satellite lines due to the coupling with ^{29}Si (I = ½, 4.7% natural abundance) can be observed in EPR spectra of silyl radical spin adducts of PBN, provided a sufficient signal-to-noise ratio [37]. In 2008, a new class of type I silyl-based photo-initiators was designed by Lalevée and co-workers for FRP applications [39]. In this study, EPR–ST highlighted new photochemical mechanisms involving Si–Si bond cleavage by energy transfer reaction with the excited triplet state of BP. The radical species were clearly ascribed to silyl radical adducts, which possess very high a_N and a_H values: trialkylsilyl radical (a_N = 14.8 G, a_H = 6.1 G) and *tris*(trimethylsilyl)silyl radical (TMS)$_3$Si$^\bullet$ (a_N = 15.3 G, a_H = 5.5 G). A similar investigation was proposed by using new silyloxyamines derived from pentamethyldisilane [40], the absorption properties of which were tuned by introducing localized p systems, favouring their polymerization initiation ability. By simple irradiation, an Si–Si bond cleavage was observed and resulted from a significant electron transfer from the julolidine group to the silyl ether group, leading to trimethylsilyl radical adducts of PBN (a_N = 14.8 G, a_H = 6.3 G). Interestingly, such compounds proved they could be used also as type II photo-initiators when combined with photosensitizers such as BP. Indeed, due to the bond dissociation energy (BDE) of Si–Si being lower than the energy of the BP triplet excited state (^{3}BP), the energy transfer process favours the Si–Si bond cleavage as demonstrated by EPR–ST. In line with these considerations, a series of silane-derived systems (R$_3$Si-H) associated with BP [53] was described as efficient photocatalyst systems for increasing free-radical photopolymerization of acrylate monomers under air. R$_3$Si-H behaves as a high-performance co-initiator to form silyl radicals (R$_3$Si$^\bullet$) by the H-abstraction reaction, which is capable of reducing the detrimental oxygen inhibition effect by forming peroxyl radicals (R$_3$SiOO$^\bullet$) and allowing for R$_3$Si$^\bullet$ renewal. Interestingly, the combination of silane-based molecules, iodonium salt, and CQ represents a remarkable redox free-radical and cationic photo-initiating system. In its excited state, CQ abstracts hydrogen from silane-based compounds to form not only silyl radicals able to initiate FRP under air but also the oxidized form of silyl radicals (silylium ion, R$_3$Si$^+$) involved in cationic photopolymerization. Similar systems were used in oxidative photocatalysis [54]. Indeed, iridium(III) complexes (Ir) were used as efficient photoinitiators for FRP in combination with an iodonium salt (i.e., diphenyliodonium hexafluorophosphate, Ph$_2$I$^+$)

and silane derivatives (R$_3$Si-H). The iridium excited state reacts with Ph$_2$I$^+$ to generate both the oxidant metal complex (Ir$^+$) and phenyl radicals. The later are involved in a hydrogen abstraction process with R$_3$Si-H to yield R$_3$Si$^\bullet$, which is further oxidized by Ir$^+$, leading thus to the regeneration of Ir and the formation of cationic species (silylium ion, R$_3$Si$^+$). Such an oxidative photoredox catalysis can therefore be employed for FRP and cationic polymerization in the visible range. The same reactions were proposed for CP at long wavelengths and under air in the presence of *bis*(cyclopentadienyl)bis[2,6-difluoro-3-(1-pyrryl)phenyl]titanium Ti, a silane (*tris*(trimethylsilyl)silane TTMSS), and a iodonium salt [55]. The involved mechanisms during photolysis of this photo-initiating system were clearly detailed by EPR. This technique evidenced the formation of a titanium-centred radical (g = 1.978), and, in the presence of PBN, the formation of the (TMS)$_3$Si$^\bullet$ radical was proven by the detection of the adduct characterized by HFS a$_N$ = 15.2 G and a$_H$ = 5.5 G in *tert*-butylbenzene. EPR–ST proved the absence of cyclopentadienyl and benzyl radicals, suggesting an H-abstraction reaction between those radicals and TTMSS to generate silyl radical. The gradual decrease of silyl radicals over time evidenced the formation of silylium ion (R$_3$Si$^+$) involved in CP.

3.2.3. Boryl Radical Spin Adducts of PBN in FRP

In 2010, boryl chemistry was the field of revived interest, and thereby the efficiency of a new class of radicals derived from *N*-heteroaryl boranes was investigated. Interestingly, the low B-H BDE (around 80 kcal.mol^{-1}) permits these borane derivatives to be used as co-initiators for the type II photopolymerization of acrylates with BP [56]. Under light irradiation, ketyl radicals, generated from the hydrogen abstraction of borane derivatives by ^{3}BP, and boryl radicals were concomitantly produced. The high nucleophilic character of the photoinduced boryl radicals was associated with a high addition rate constant to acrylates, leading thus to high final conversions, even under air. Such a reaction was strictly confirmed by EPR–ST. Both natural boron isotopes are characterized by a non-zero nuclear spin I(^{11}B) = 3/2 (80% natural abundance) and I(^{10}B) = 3 (20%) and induce additional HFS in the spectra of PBN spin adducts of boryl radicals. However, in most studies, only the ^{11}B coupling is resolved and simply referred to as a$_B$. For instance, the HFS constants were as follows: a$_N$ were comprised between 15.1 and 15.2 G, and a$_H$ were in the range 2.1–2.8 G and 3.5 < a$_B$ < 4.7 G, in good agreement with previous results on other boryls [57]. More recently, similar results were obtained with *N*-heterocyclic carbene (NHC) complexes of boranes [58] used as a new class of co-initiators for the type II polymerization of acrylates under light irradiation in the 300–350 nm range. The formation of the NHC-boryl radicals was easily established by EPR–ST experiments: the expected spin adducts of the NHC-boryl radical were characterized by a$_N$ ~15.4 G, a$_H$ ~2.1 G, and a$_B$ ~4.4 G, thereby confirming the intended H abstraction reaction process. In light of these results, a series of *N*-heterocyclic carbene−boryl sulfides (NHC-BS) [41] was designed to efficiently perform FRP under air. Remarkably, NHC-BS can play a dual role as a type I photo-initiator and as a co-initiator in a type II photo-initiating system. EPR–ST with PBN in *tert*-butylbenzene clearly demonstrated that NHC-BS could be involved in a homolytic B-S bond cleavage when irradiated under UV light. The resulting EPR–ST spectra are considered as the sum of signals from the NHC-boryl or NHC-thioboryl radical adducts and the thiyl radical (PhS$^\bullet$ or NaphthylS$^\bullet$) adduct in different proportions (Figure 8). NHC-boryl and NHC-thioboryl radical adducts revealed three significant hyperfine coupling constants, i.e., 15.1 < a$_N$ < 15.2 G, 2.1 G < a$_H$ < 3.1 G, and 4.2 G < a$_B$ < 4.6 G; the HFS characteristic of the resulting PhS$^\bullet$/PBN radical adduct were determined to be a$_N$ = 13.9 and a$_H$ = 1.8 G. Remarkably, NaphthylS$^\bullet$ was not trapped by PBN, which means that its addition rate to PBN was slower than that observed with boryl radicals. Interestingly, when NHC-BS were used as co-initiators with BP, the same boryl radical adducts were identified following an H-abstraction reaction process.
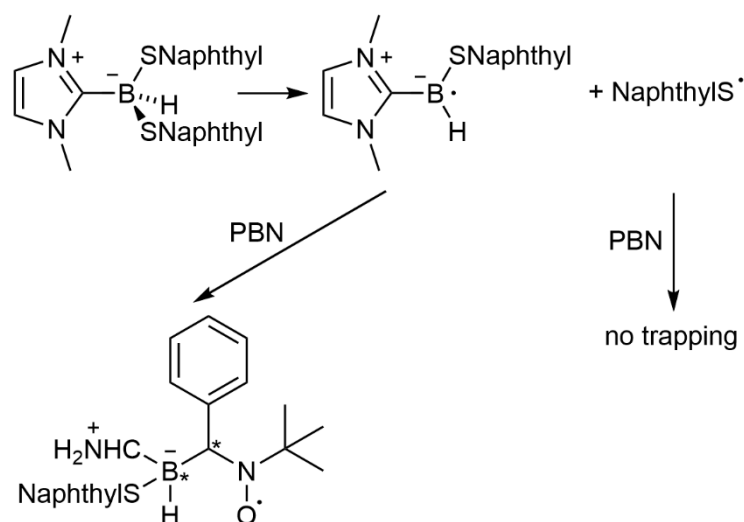
Figure 8. PBN spin adducts derived from an NHC-boryl bis-sulfide photopolymerization initiator [41]. The two stereogenic centres in the spin adduct are identified with asterisks.

3.2.4. Phosphinoyl Radical Spin Adducts of PBN

In recent decades, *bis*(acyl)phosphine oxides have gained great attention in polymerization [59,60] because of their high and efficient photo-initiating properties in free-radical photopolymerization and due to the extension of their absorbance into the visible range. The phosphinoyl radicals generated under UV irradiation are used both in FRP and in free radical-promoted cationic photopolymerization (FRPCP). Particularly, Turro was the first to study the photochemical behaviour of a series of bis(acyl)phosphine oxides under light irradiation, thereby correlating in detail the reactivity of phosphinoyl radicals towards oxygen, thiophenol, methyl viologen, or acrylate monomers with the degree of radical localization on the phosphorus atom by time-resolved EPR [60]. In 1997, Sueishi et al. observed the reactivity of diphenylphosphinyl radical ($\bullet$PPh$_2$) toward different kinds of spin-traps in benzene, particularly with PBN. Based on the g value (2.0060) and the hyperfine coupling structure of the EPR spectra ($a_P = 18.2$ G, $a_N = 14.1$ G, $a_H = 3.2$ G), the phosphinyl radicals were considered as the main radical trapped by PBN. The spin adduct PBN-PPh$_2$ displays a large characteristic doublet caused by the phosphorus atom [61]. More recently, the photosensitized decomposition of new phosphorus-containing compounds (R'$_2$P-OR or R$_2$P(=O)-H) by BP (or other photosensitizers such as isopropylthioxanthone, eosin, or CQ) was investigated, and an overview of the reactivity of the generated phosphorus-centred radicals [62] was reported. EPR–ST clearly evidenced a two-step process for R'$_2$P-OR compounds. First, the formation of the phosphoniumyl radical ion R'$_2$P$^{\bullet+}$−OR occurs through an electron transfer reaction between the photosensitizer and R'2P-OR followed by the fragmentation of the phosphoniumyl radical ion into a phosphinoyl radical R'$_2$P$^{\bullet}$(=O). The second reaction involves a hydrogen abstraction reaction from the P−H bond of R$_2$P(=O)-H using the suitable photosensitizer. The HFS of the phosphorus-centred radical adducts using PBN were $14.2 < a_N < 14.5$ G, $2.9 < a_H < 3.1$ G, and $19.1 < a_P < 25.2$ G and agree with the literature. Recently, Versace et al. designed a new vanillin-derived type I photoinitiator [63] based on phosphine oxide (4-allyloxy-3-methoxybenzoyl)diphenylphosphine oxide; PM). According to Turro's studies, this new kind of photoinitiator should undergo a carbon-phosphorus bond homolytic photocleavage to yield benzoyl and phosphinoyl radicals, which should be readily observable at around 330 nm by laser flash photolysis (LFP). Unfortunately, the LFP signals of both expected radicals were merged between 320 and 380 nm. Therefore, the identification of non-persistent radical species upon irradiation of PM was carried out by EPR–ST using PBN, and four main EPR signals from two phosphinoyl and two carbon-centred radicals were identified. One must underline that the signal intensities of the PBN spin adducts of phosphinoyl-derived radicals are higher than

those of benzoyl radicals due to their faster rate of addition on PBN and their lower rate of relaxation compared to that of benzoyl radicals [33].

3.2.5. Other PBN-Radical Adducts

Thiyl radical adducts of PBN are usually poorly stable or hardly distinguishable [64], except in some specific cases. The phenylthiyl radical adduct of PBN is well-known [65] (a_N = 13.9 G, a_H = 1.8 G in benzene) and has been detected in the photolysis of a NHC–BS photo-initiator [41]. Interestingly, Versace et al. also observed thiyl radicals by the direct UV-irradiation of trimethylolpropane tris(3-mercaptopropionate) (TT)/DMPA photo-initiating system in *tert*-butylbenzene [12]. In non-aerated medium, DMPA leads to the formation of benzoyl radicals (a_N = 14.1 G and a_H = 4.4 G), which abstract hydrogen from TT to induce thiyl radicals (a_N = 13.9 G and a_H = 2.2 G).

3.3. Cyclic Nitrone Spin Traps

Cyclic nitrone spin traps usually yield spin adducts with more characteristic EPR spectra than PBN thanks to a larger and more structure-sensitive $a_{H\beta}$ value. Moreover, additional small couplings with one or two hydrogen nuclei in the γ-position to the nitrogen in the ring may sometimes appear on the spectra. DMPO, being the historical spin trap and commercially available, is the most frequently used and benefits from an abundant literature. A β-phosphorylated analogue, DEPMPO (5-diethoxyphosphoryl-5-methyl-1-pyrroline *N*-oxide) [66,67], has been developed to facilitate the attribution of the EPR signal with an additional ^{31}P hyperfine coupling and is also frequently used. In a seminal study, DMPO was applied systematically to the study of various types of PIS in comparison to PBN [30]. It afforded satisfactory detection of alkyl-, aminoalkyl-, aryl-, ketyl-, thiyl-, and phosphorus-centred radicals [30,36].

3.3.1. α-Aminoalkyl Radical Spin Adducts of DMPO

In the 2000s, the trapping of aminoalkyl radicals by DMPO was very scarce in the literature due to the difficulties in producing these high performing and initiating radicals. Nowadays, α-aminoalkyl radicals have been successfully generated by an electron transfer process following the H-abstraction reaction between MDEA (an electron donor molecule) and a photosensitizer. Numerous interesting studies have been published, and a series of photosensitizers, i.e., natural dyes; CQ; and anthraquinone-, thioxanthone-, porphyrin-, or phthalocyanin-derivatives have been therefore proposed [18,20,22,68,69]. The structure of the α-aminoalkyl radical strongly influences HFS when using DMPO, and the latter appears less selective than PBN in the trapping of these radicals (Criqui et al. 2008). Recently, Versace et al. reported the use of new visible-light-absorbing thioxanthone derivatives [69] with effective initiating properties when associated with MDEA upon irradiation at 405, 455, and 470 nm with light-emitting diodes (LEDs). Interestingly, these systems prove to successfully promote the FRP, even under air, thanks to the formation of α-aminoalkyl radicals. The generation of the dominant EPR–ST signal fully compatible with the α-aminoalkyl radical DMPO-adduct is characterized by the following HFS in benzene: a_N = 14.73 G, $a_{H\beta}$ = 18.1 G, $a_{H\gamma}$ = 0.9 G; g = 2.0060. Similar results were obtained with the photoexcitation of purpurin derivatives/MDEA systems [35] in the presence of a DMPO spin trapping agent in benzene. The α-aminoalkyl radical DMPO-adduct shows HFS parameters as follows: a_N = 14.61 G, $a_{H\beta}$ = 17.88 G, $a_{H\gamma}$ = 1.15 G; g = 2.0058. The later HFS parameters evolve when a spin-trapping reaction occurs in dimethylsulfoxide (DMSO). For instance, irradiation of methacrylated quinizarin/MDEA systems [18] in the presence of DMPO in DMSO leads to the following HFS parameters: a_N = 14.66 G, $a_{H\beta}$ = 19.45 G, $a_{H\gamma}$ = 0.62 G; g = 2.0059. These are slightly different to what was previously described in non-polar solvent.

3.3.2. Thiyl Radical Spin Adducts of DMPO

The thiol-ene process under light irradiation has been extensively studied over the last century. As evidenced by the high number of investigations, thiol-ene technology continues to grow, and numerous striking advantages [70,71] could be underlined such as low shrinkage, high ene final conversions with fast polymerization rates, insensitivity to oxygen, and uniform crosslink densities. The generated flexible thioether linkages during the thiol-ene process provide high heat resistance, low water absorption, and low oxidation susceptibility to the resulting materials. Interestingly, high storage moduli have been observed in the glassy thiol-ene-based materials, even when subjected to deformation. More recently, various thiol–acrylate systems have been investigated and have demonstrated their capability to produce thick materials, even after irradiation under air, establishing the further great potential of thiol-ene chemistry in future applications. This technology is well-known to occur through a free-radical step-growth mechanism involving a two-step process: at the early stage, thiyl radicals add on the carbon of an ene functionality to give carbon-centred radicals. Subsequently, a hydrogen abstraction reaction occurs between the thiol group and the carbon-centred radical to form a thiyl radical. Finally, a radical–radical coupling ends the polymerization. For instance, investigations [35] with TT, soya bean oil acrylate, and purpurin derivatives demonstrated that the kinetics of acrylate photopolymerization were moderately slowed down under air; the generated thiyl radicals trap oxygen to form peroxyl radicals ($RSOO^\bullet$), which are subsequently involved in a proton transfer reaction with TT, thus regenerating the thiyl radicals. Thiyl radicals have been experimentally observed after being trapped by DMPO, and the spin-Hamiltonian parameters extracted from the simulation of EPR spectra (i.e., a_N = 13.47 G, $a_{H\beta}$ = 11.73 G, $a_{H\gamma}$ = 0.90 G, $a_{H\gamma}$ = 0.97 G; g = 2.0061 in benzene) are attributed to the DMPO-adduct with the thiyl radical. Similar results were recently obtained with di-methacrylated quinizarin dyes/TT photoinitiating systems [18] upon LED irradiation at 405 nm; two EPR signals were immediately observed, i.e., one attributed to the quinizarin radical anion along with the $RS^\bullet$/DMPO spin adduct. Interestingly, the HFS of the thyil radical spin adduct were a_N = 13.80 G, $a_{H\beta}$ = 13.19 G, $a_{H\gamma}$ = 0.87 G, $a_{H\gamma}$ = 0.70 G, g = 2.0061 in DMSO.

3.3.3. Phosphorus-Centred Radical Spin Adducts of DMPO

Only a few investigations reported the spin-trapping of phosphorus-centred radicals [61,72]. In the study of Nishihara et al., the spin-trapping efficiency of diphenylphosphinyl radical ($^\bullet PPh_2$) with some spin traps (PBN, DMPO) were reported, and the trapping rates of this radical were studied by competitive reactions [36]. Interestingly, it was proven that the spin trapping of $^\bullet PPh_2$ by DMPO is less favourable than that by PBN. Extrapolating from molecular calculations [73,74] and their kinetics observations, the authors concluded that the $^\bullet PPh_2$ radical behaves as a nucleophile upon addition to the nitrone. The pattern of the EPR signal of the $^\bullet PPh_2$/DMPO spin adduct is similar to what can be obtained with PBN. However, the $^\bullet PPh_2$/DMPO spin adduct exhibits remarkably large HFS (a_P = 37.2 G, a_N = 13.6 G, a_H = 18.3 G), compared with those of PBN-adducts (a_P = 18.2 G, a_N = 14.1 G, a_H = 3.2 G) in benzene [61]. More recently, Criqui et al. [30] failed to observe phosphinoyl radicals generated from the photolysis of phosphine oxide-based photo-initiators. The nucleophilic addition of these radicals onto DMPO was not thermodynamically favoured to be easily observed.

3.3.4. (4-Methyl)phenyl Radical Spin Adduct of DMPO

Phenyl derived radicals generated from the photolysis of iodonium salts by electron transfer reactions have demonstrated high reactivity toward acrylate double bonds for the initiation of free-radical polymerization upon visible LED irradiation [19,35]. However, few investigations have described the spin-trapping of (4-methyl)phenyl radical by DMPO. For instance, a chlorophyll *a* derivative and its corresponding zinc (II) complex [19] were employed as efficient visible-light photosensitizers for free-radical photopolymerization of multi-acrylate monomer when associated with an oxidizing agent, i.e., (4-methylphenyl) [4-

(2-methylpropyl)phenyl] iodonium hexafluorophosphate (a iodonium salt). A six-line EPR signal associated with the spin-Hamiltonian parameters, namely, a_N = 14.54 G, a_H = 21.34 G, and g = 2.0059, is well compatible with the (4-methyl)phenyl spin adduct of DMPO in acetonitrile solution. The HFS of the (4-methyl)phenyl/DMPO spin adduct elucidated from the experimental EPR spectra obtained upon irradiation of purpurin derivatives/Iod in benzene solutions were slightly different to those observed in acetonitrile with a_N = 14.02 G, a_H = 19.55 G, and g = 2.0060 [35].

4. Experimental Setup

4.1. Solvent and Cell Choice

The solvent must dissolve all the components of the spin trapping experiment. In addition, solvents with high dielectric constants, such as acetonitrile, require the use of flat cells, an AquaX® cell (Bruker, Billerica, MA, USA), or capillary tubes because they otherwise induce non resonant absorption of the microwave and prevent tuning of the spectrometer [75]. Otherwise, 4-mm cylindrical quartz tubes can be used to prepare the samples. A lot of HFS data was originally obtained in benzene in the literature [76], but it is preferable to substitute this carcinogenic solvent in future studies. Some solvents, such as dimethylformamide, should be avoided in spin trapping experiments because they enhance nucleophile addition to nitrones, which can lead to artefactual formation of nitroxide through the Forrester–Hepburn mechanism (see Section 5.3).

4.2. Spin Trap Concentration

Precise concentrations of reaction components are often not reported in research articles on PIS, as only qualitative information is targeted. The spin trapping reaction is in competition with other reactions of the investigated radicals, such as radical recombination or fragmentation. Enough spin trap must thus be introduced at the start of the radical production. However, the spin trap concentration must not be too high to reduce the internal filtering of the excitation wavelength when it falls in the spin trap absorption range. High nitrone spin trap concentrations have also been shown to reduce the stability of spin adducts [29]. Concentrations of the spin trap ranging from 1 mM to 100 mM are used, 20–50 mM being the optimal range in most studies. With such concentrations, contamination of the spin trap by traces of hydroxylamine or nitroxide impurities can lead to artefactual signals in the spectra and misinterpretation. It is thus important to regularly check the purity of the batch used. Contaminating hydroxylamines can be tested by treatment with ferricyanide, which converts them to EPR-visible nitroxides [77]. DMPO has a reduced shelf-life and often contains paramagnetic impurities. DEPMPO is usually more stable upon long-term storage at −20 °C or lower, but it can also become contaminated. Both being oils at room temperature, they are difficult to purify by distillation on a small scale. PBN, on the contrary, has a long shelf-life and can be purified by recrystallization.

4.3. Removal of Oxygen

Oxygen is a well-known inhibitor of many radical polymerization processes because the formation of secondary radicals occurs. This is a first reason why the PIS samples are usually degassed with nitrogen or argon. A second reason is the broadening induced by oxygen, a paramagnetic biradical in its ground state, on the EPR spectrum. Degassing enables better observation of the hyperfine structure of the spectra [53].

4.4. Irradiation In Situ or Ex Situ

Some EPR cavities are equipped with irradiation windows that allow irradiation in situ during EPR acquisition. This is mandatory for the study of very short-lived spin adducts such as the PBN adducts of phosphinoyl radicals [33]. Caution must be taken not to damage the cavity by overheating with high energy radiation, and it is good practice to verify the stability of the spin trap under the conditions of study. Depending on the system under study and providing sufficient stability of the spin adducts formed, ex situ

irradiation is an alternative. Heating of the sample induced by infrared light irradiation greatly alters the kinetics of the spin trapping reaction and reduces the spin adduct lifetime, which can impair detection.

4.5. Acquisition Parameters

Acquisition parameters are critical to afford detection of low and transient concentrations of spin adducts. Microwave power between 10 and 20 mW is widely accepted to optimize EPR intensity while avoiding saturation of the signal for nitroxides [78]. Modulation of the magnetic field is used in conventional spectrometers to enhance the sensitivity of EPR acquisition, which results in the EPR spectrum being recorded as the first derivative of the absorption signal. Recommended modulation amplitude is generally around 0.1 mT for nitroxides, but lower values up to 0.01 mT can be chosen to better resolve small hyperfine structure or higher values up to 0.25 mT to detect low signals. When looking at weak signals, a further increase in signal-to-noise ratio can be accessed by using large time constants to reduce noise or by repeatedly acquiring the spectrum and subsequently adding the spectra together. As a result, the signal increases proportionally with the number of scans N, random noise with $\sqrt{N}$, and thus signal-to-noise ratio with $\sqrt{N}$. Modern spectrometers also allow automatic sequential recording of large series of spectra, and this function can be used to further increase the sensitivity of detection with spin traps. Application of data processing methods to large series of spectra, such as singular value decomposition (SVD), can afford extraction of kinetic information in addition to noise filtration [29].

5. Interpretation of Results

5.1. Signal Attribution

Once EPR spectra have been recorded, attribution of the signal to specific radical species involves extraction of hyperfine coupling constants. A lot of information can be obtained from careful examination of the spectra [32]. When approximate values of the parameters have been determined, more precise values are derived from fitting of a calculated spectrum to the experimental data with the help of numerical simulation software. In spin trapping experiments, the most popular programs are WinSim [79], made freely available to the EPR community by NIEHS at https://www.niehs.nih.gov/research/resources/software/tox-pharm/tools/index.cfm (accessed on 12 May 2022), and EasySpin, a dedicated MATLAB toolbox [80]. A correctly performed simulation requires optimization of the following variables for each radical species: a_N and the HFS for additional coupling nuclei, the relative weight of each species in the spectrum, the g-value, the linewidth, and the Lorentzian component of the lineshape. The number of variables rises thus very quickly when mixtures of adducts are detected, making the simulation a very challenging task. One must be careful not to overinterpret the results of numerical simulation.

The trapped radical can be identified by comparing the HFS values deduced from the analysis of the spectrum to those from the literature, considering they may slightly vary depending on the nature of the solvent. Useful compilations of HFS are found in the work by Buettner [76] and in the online NIEHS database https://tools.niehs.nih.gov/stdb/index.cfm (accessed on 12 May 2022).

The HFS for new spin adducts that are not found in the literature can be confirmed by carrying out control spin trapping experiments in which the same radical is formed by a different method. This strategy was followed to characterize unambiguously the silyl radical produced from novel photo-initiators and trapped with PBN [39].

Formation of the diastereomeric nitroxide spin adduct (bearing two stereogenic centres) may result from the radical trapping reaction. This can translate into different EPR spectra, because of differences in the interactions between substituents [81], and further add to the complexity of interpretation. The difference between the spectra of diastereomers may be so small that only one set of HFS is observed, as in the PBN spin adducts derived from NHC-boryl bis-sulfide photopolymerization initiators [41] (Figure 8).

In the case of very intense spectra, small satellite lines can be observed due to hyperfine coupling to ^{13}C (I = ½, 1% natural abundance) and, less likely, ^{15}N (I = ½, 0.4% natural abundance). They can be used to confirm the attribution of the signal by simulation (Figure 9) [35].
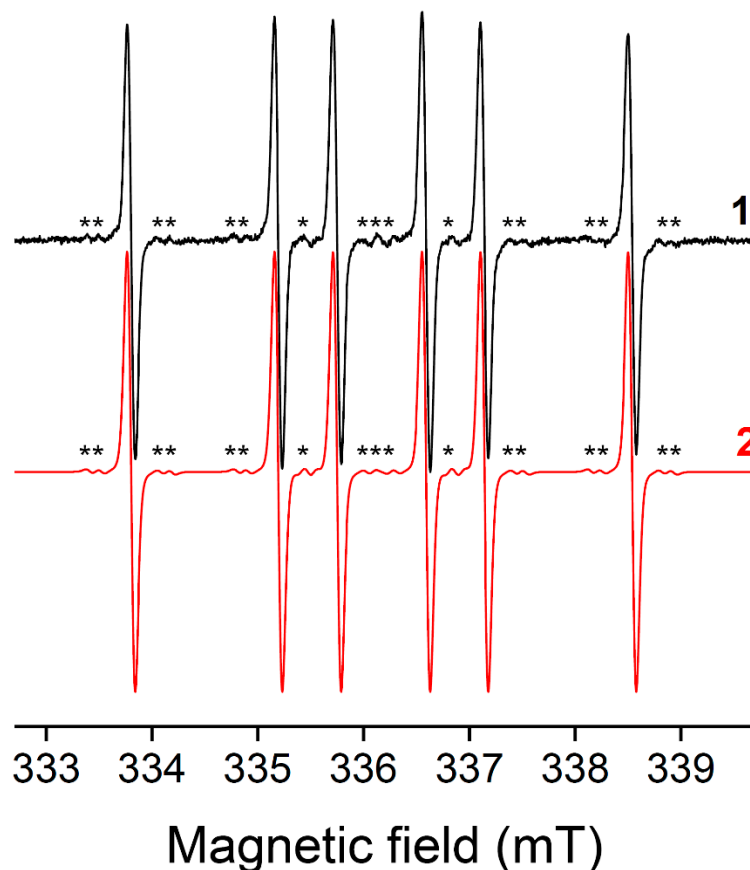

Figure 9. Experimental (1) and simulated (2) EPR spectra of the (4-methyl)phenyl radical spin adduct of DMPO obtained upon LED irradiation at 400 nm of allylated purpurin and Iod in benzene under argon. Satellite lines due to hyperfine coupling to ^{13}C are indicated with asterisks. Reproduced from Ref. [35]. Copyright 2021 permission Royal Society of Chemistry.

5.2. Kinetic Considerations

Assuming the recording parameters have been properly chosen to avoid saturation of the EPR signal, the intensity of the spectrum is proportional to the number of spins in the sample, and the concentration of the spin adduct can easily be deduced from the comparison with an external standard of known concentration (usually a stable nitroxide). Considering that the spin trapping rate and the stability of spin adducts highly depend on the radical under study, it is dangerous to draw conclusions about the relative proportions of trapped radicals upon simultaneous detection of multiple spin adducts (see also Section 5.3). For example, the intensity of PBN spin adducts of benzoyl radicals detected from a vanillin-derived type I photoinitiator was much smaller than that of phosphinoyl radicals, despite their concomitant formation by homolytic cleavage of the carbon–phosphorus bond [63]. This can be rationalized by the published spin trapping rates [33] ($k_{benzoyl/PBN} = 8 \times 10^5$ M^{-1} s^{-1} vs. $k_{phosphinoyl/PBN} = 3 \times 10^7$ M^{-1} s^{-1}).

Formation of a radical in a PIS under irradiation should thus not be discarded on the basis of unsuccessful EPR detection using spin traps. A low spin trapping rate or the high instability of the spin adduct can prevent accumulation of the signal above EPR detection limit. For example, stabilized dimethoxybenzyl radicals are not trapped by PBN in EPR–ST studies, but their characteristic absorption at 410 nm can be readily observed

in LFP experiments during the photolysis of di-*tert*-butylperoxide benzaldehyde dimethy-lacetal [30]. Similarly, the highly stable iminyl radicals formed upon the photocleavage of the acyloxime photobase (*Z*)-*7H*-benzo[de]anthracen-7-one *O*-(2-phenylacetyl)oxime are not detected with PBN, even if homolytic cleavage of the N–O bond followed by a fast decarboxylation is confirmed by the detection of benzyl radical adducts (a_N = 14.3 G, a_H = 2.5 G in *tert*-butylbenzene) [30].

5.3. Potential Artefacts

On the other hand, reactions that do not involve radical trapping may lead to ni-troxides and false positive results. Specific warnings against misinterpretations appeared in the literature, mainly in the field of biological applications [82,83]. Possible artefacts comprehend: (a) oxidation of DMPO and related nitrones to the corresponding hydroxamic acid by oxidants, followed by oxidation to a nitroxide characterized by a 7-line EPR spec-trum [84]; (b) inverted spin trapping [85–87]; and (c) the Forrester–Hepburn mechanism [88] (Figure 10). The latter two reactions lead to radicals that are identical to spin adducts but through combinations of mono-electronic oxidation of the spin trap and nucleophilic addi-tion, in either order. The oxidation potentials of the spin traps must be compared to those of the PIS components to exclude the possibility of inverted spin trapping in the presence of strong oxidants ($E_{PBN\bullet+/PBN} \approx 1.7$ V and $E_{DMPO\bullet+/DMPO} \approx E_{DEPMPO\bullet+/DEPMPO} \approx 2.1$ V vs. SHE) [86,89,90]. The Forrester–Hepburn mechanism, where the first step involves nucleophilic attack of the nitrone by a nucleophile and formation of a readily-oxidizable hydroxylamine product, is potentially a greater source of artefacts [91], especially when studying thiol-ene photopolymerization initiation processes with high thiol concentrations. Indeed, EPR signals similar to that resulting from trapping of thiyl radicals by DMPO are observed even in the absence of irradiation due to this process. Under irradiation, an increase of the EPR signal of the thiyl adduct could result from the photo-induced oxidation of preformed hydroxylamine, independently of the formation of genuine thiyl radicals (Figure 11). Confirmation of the formation of thiyl radicals by another technique is crucial here to conclude.

(a) Formation of DMPOX
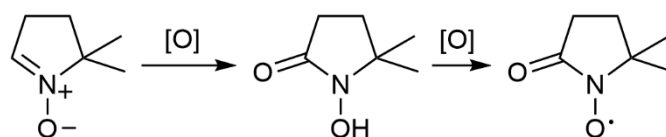
(b) Inverted spin trapping
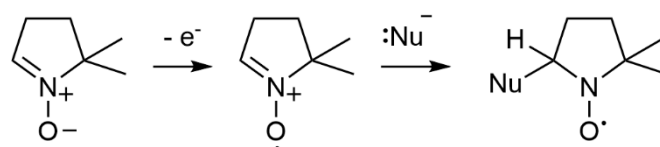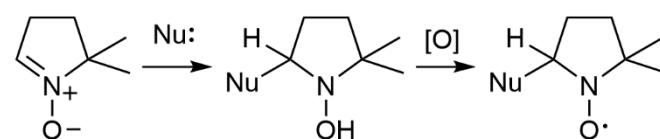

(c) Forrester-Hepburn mechanism

Figure 10. Pathways leading to artefactual detection of nitroxides in spin trapping experiments: (**a**) formation of the DMPOX nitroxide characterized by a 7-line EPR spectrum under oxidizing conditions; (**b**) inverted spin trapping; and (**c**) Forrester-Hepburn mechanism. DMPO is used as a model spin trap in this figure, but similar mechanisms exist for other nitrones. [O] stands for the oxidation step, and Nu: for nucleophiles such as thiols.
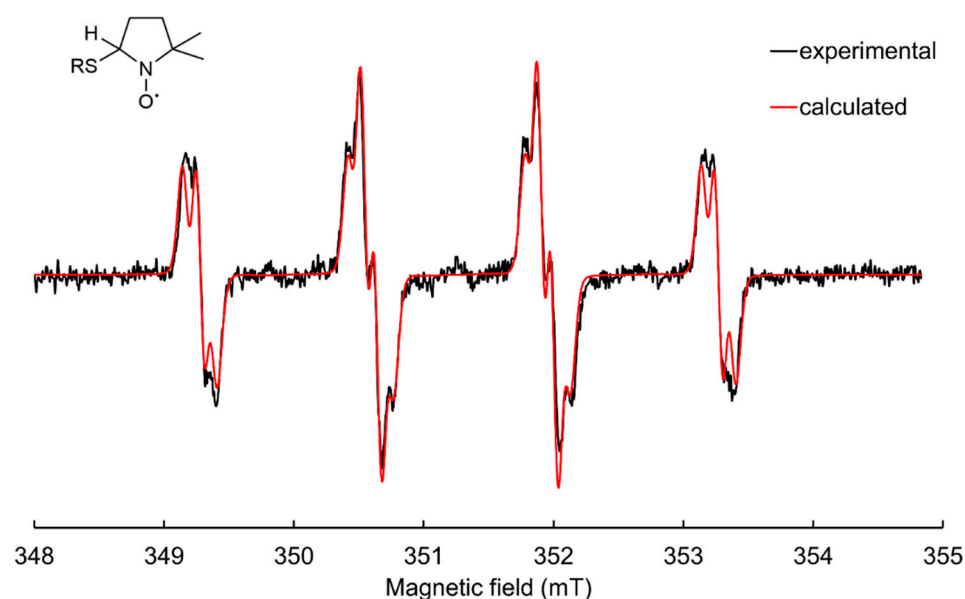
Figure 11. EPR signal observed in dichloromethane in the presence of DMPO and TT (~50 and 400 mM, respectively) in the absence of any light irradiation and resulting from the Forrester–Hepburn mechanism. The red trace corresponds to the EPR simulation using the following parameters: a_N = 13.6 G, $a_{H\beta}$ = 12.8 G, $a_{H\gamma}$ = 0.9 and 1.1 G, and g = 2.0061, indistinguishable from that observed when trapping thiyl radicals.

6. Conclusions

EPR–ST is now widely recognized as the gold standard to support the identification of short-lived radicals produced under photoirradiation of PIS developed for photopolymerization. It is complementary to other techniques that yield more direct information, such as LFP coupled to UV–visible absorption spectroscopy and spectroelectrochemistry. Indeed, LFP allows short or long-lived radical species, which absorb in the visible range, to be detected easily; however, these are much more difficult to detect when absorption occurs in the UV range, where LFP signals of many radicals can merge, and when absorption coefficients of radicals are low. A limited number of spin traps has been used in PIS studies, mainly PBN and DMPO, while a large variety of structures has been designed and applied successfully in other fields of in-solution chemistry [28]. β-Phosphorylated analogues, PPN and DEPMPO, are especially interesting because the additional ^{31}P hyperfine interaction facilitates the identification of the trapped species. In experimental plans, including several spin traps to study the mechanism of new PIS is critical in order not to miss important radicals, since a certain selectivity can be observed. One must be fully aware of the advantages of the method but also of its limitations when designing the spin trapping experiment, including appropriate controls, and when interpreting the results.

Author Contributions: Conceptualization, D.-L.V. and F.P.; methodology, D.-L.V. and F.P.; validation, D.-L.V. and F.P.; investigation, D.-L.V., S.L. and F.P.; writing—original draft preparation, D.-L.V. and F.P.; writing—review and editing, D.-L.V. and F.P.; visualization, D.-L.V., and F.P.; supervision, D.-L.V. and F.P. All authors have read and agreed to the published version of the manuscript.

Conflicts of Interest: The authors declare no conflict of interest.

Abbreviations

BDE	bond dissociation energy
BP	benzophenone
CP	cationic photopolymerization
CQ	camphorquinone
DEPMPO	5-diethoxyphosphoryl-5-methyl-1-pyrroline *N*-oxide
DMPA	2,2′-dimethoxyphenyl acetophenone
DMPO	5,5-dimethyl-1-pyrrolidine *N*-oxide
DMSO	dimethylsulfoxide
EPR	electron paramagnetic resonance
ESR	electron spin resonance
FRP	free radical photopolymerization
FRPCP	free radical promoted cationic photopolymerization
HFS	hyperfine splitting
Iod	bis(4-methylphenyl) iodonium hexafluorophosphate
Ir	iridium(III) complexes
LED	light-emitting diode
LFP	laser flash photolysis
MDEA	*N*-methyl diethanol amine
MNP	1-methyl-1-nitrosopropane
ND	nitrosodurene
NIR	near infrared
NHC	*N*-heterocyclic carbene
NHC-BS	*N*-heterocyclic carbene-boryl sulfide
NP	nanoparticle
PBN	*N*-*tert*-α-phenyl-butylnitrone
PIS	photo-initiating system
PM	4-allyloxy-3-methoxybenzoyl)diphenylphosphine oxide
PPN	diethyl 1-(*N*-benzylidene *N*-oxyamino) 1-methylethyl phosphonate
ST	spin trapping
SVD	singular value decomposition
TT	trimethylolpropane *tris*(3-mercaptopropionate)
TTMSS	*tris*(trimethylsilyl)silane

References

1. Pierau, L.; Elian, C.; Akimoto, J.; Ito, Y.; Caillol, S.; Versace, D.-L. Bio-sourced monomers and cationic photopolymerization–The green combination towards eco-friendly and non-toxic materials. *Prog. Polym. Sci.* **2022**, *127*, 101517. [CrossRef]
2. Pierau, L.; Versace, D.-L. Light and Hydrogels: A New Generation of Antimicrobial Materials. *Materials* **2021**, *14*, 787. [CrossRef] [PubMed]
3. Fouassier, J.-P.; Lalevée, J. *Photoinitiators for Polymer Synthesis: Scope, Reactivity and Efficiency*; Wiley-VCH Verlag GmbH & Co. KGaA: Weinheim, Germany, 2012.
4. Bao, Y.; Paunović, N.; Leroux, J. Challenges and Opportunities in 3D Printing of Biodegradable Medical Devices by Emerging Photopolymerization Techniques. *Adv. Funct. Mater.* **2022**, *32*, 2109864. [CrossRef]
5. Versace, D.-L.; Breloy, L.; Palierse, E.; Coradin, T. Contributions of photochemistry to bio-based antibacterial polymer materials. *J. Mater. Chem. B* **2021**, *9*, 9624–9641. [CrossRef] [PubMed]
6. Versace, D.-L.; Ramier, J.; Grande, D.; Andaloussi, S.A.; Dubot, P.; Hobeika, N.; Malval, J.-P.; Lalevee, J.; Renard, E.; Langlois, V. Versatile Photochemical Surface Modification of Biopolyester Microfibrous Scaffolds with Photogenerated Silver Nanoparticles for Antibacterial Activity. *Adv. Health Mater.* **2013**, *2*, 1008–1018. [CrossRef]
7. Breloy, L.; Ouarabi, C.A.; Brosseau, A.; Dubot, P.; Brezova, V.; Andaloussi, S.A.; Malval, J.-P.; Versace, D.-L. β-Carotene/Limonene Derivatives/Eugenol: Green Synthesis of Antibacterial Coatings under Visible-Light Exposure. *ACS Sustain. Chem. Eng.* **2019**, *7*, 19591–19604. [CrossRef]
8. Versace, D.-L.; Moran, G.; Belqat, M.; Spangenberg, A.; Méallet-Renault, R.; Abbad-Andaloussi, S.; Brezová, V.; Malval, J.-P. Highly Virulent Bactericidal Effects of Curcumin-Based μ-Cages Fabricated by Two-Photon Polymerization. *ACS Appl. Mater. Interfaces* **2020**, *12*, 5050–5057. [CrossRef]
9. Jin, M.; Hong, H.; Xie, J.; Malval, J.-P.; Spangenberg, A.; Soppera, O.; Wan, D.; Pu, H.; Versace, D.-L.; Leclerc, T.; et al. π-conjugated sulfonium-based photoacid generators: An integrated molecular approach for efficient one and two-photon polymerization. *Polym. Chem.* **2014**, *5*, 4747–4755. [CrossRef]

10. Jung, K.; Xu, J.; Zetterlund, P.B.; Boyer, C. Visible-Light-Regulated Controlled/Living Radical Polymerization in Miniemulsion. *ACS Macro Lett.* **2015**, *4*, 1139–1143. [CrossRef]

11. Fu, C.; Xu, J.; Boyer, C. Photoacid-mediated ring opening polymerization driven by visible light. *Chem. Commun.* **2016**, *52*, 7126–7129. [CrossRef]

12. Lorenzini, C.; Haider, A.; Kang, I.-K.; Sangermano, M.; Abbad-Andalloussi, S.; Mazeran, P.-E.; Lalevée, J.; Renard, E.; Langlois, V.; Versace, D.-L. Photoinduced Development of Antibacterial Materials Derived from Isosorbide Moiety. *Biomacromolecules* **2015**, *16*, 683–694. [CrossRef] [PubMed]

13. Li, L.; Scheiger, J.M.; Levkin, P.A. Design and Applications of Photoresponsive Hydrogels. *Adv. Mater.* **2019**, *31*, e1807333. [CrossRef] [PubMed]

14. Malval, J.-P.; Morlet-Savary, F.; Chaumeil, H.; Balan, L.; Versace, D.-L.; Jin, M.; Defoin, A. Photophysical Properties and Two-Photon Polymerization Ability of a Nitroalkoxystilbene Derivative. *J. Phys. Chem. C* **2009**, *113*, 20812–20821. [CrossRef]

15. Yagci, Y.; Jockusch, S.; Turro, N.J. Photoinitiated Polymerization: Advances, Challenges, and Opportunities. *Macromolecules* **2010**, *43*, 6245–6260. [CrossRef]

16. Lalevee, J.; Roz, M.E.I.; Tehfe, M.A.; Alaaeddine, M.; Allonas, X.; Fouassier, J.-P. New Opportunities in Free Radical Photopolymerization and Free Radical Promoted Cationic Polymerization Based on the Silyl Radical Chemistry. *J. Photopolym. Sci. Technol.* **2009**, *22*, 587–590. [CrossRef]

17. Andrzejewska, E.; Grajek, K. Recent Advances in Photo-Induced Free-Radical Polymerization. *MOJ Polym. Sci.* **2017**, *1*, 58–60. [CrossRef]

18. Breloy, L.; Brezová, V.; Barbieriková, Z.; Ito, Y.; Akimoto, J.; Chiappone, A.; Abbad-Andaloussi, S.; Malval, J.-P.; Versace, D.-L. Methacrylated Quinizarin Derivatives for Visible-Light Mediated Photopolymerization: Promising Applications in 3D-Printing Biosourced Materials under LED@405 nm. *ACS Appl. Polym. Mater.* **2022**, *4*, 210–228. [CrossRef]

19. Breloy, L.; Brezová, V.; Richeter, S.; Clément, S.; Malval, J.-P.; Andalloussi, S.A.; Versace, D.-L. Bio-based porphyrins pyropheophorbide *a* and its Zn-complex as visible-light photosensitizers for free-radical photopolymerization. *Polym. Chem.* **2022**, *13*, 1658–1671. [CrossRef]

20. Elian, C.; Brezová, V.; Sautrot-Ba, P.; Breza, M.; Versace, D.L. Lawsone Derivatives as Efficient Photopolymerizable Initiators for Free-Radical, Cationic Photopolymerizations, and Thiol—Ene Reactions. *Polymers* **2021**, *13*, 2015. [CrossRef]

21. Peng, X.; Yao, M.; Xiao, P. Newly Synthesized Chromophore-linked Iodonium Salts as Photoinitiators of Free Radical Photopolymerization. *Macromol. Chem. Phys.* **2021**, *222*, 2100035. [CrossRef]

22. Versace, D.-L.; Breloy, L.; Yagci, Y.; Yilmaz, I.; Yavuz, O. Design, Synthesis and Use of Phthalocyanines as a New Class of Visible-Light Photoinitiators for Free-Radical and Cationic Polymerizations. *Polym. Chem.* **2021**, *12*, 4291–4316. [CrossRef]

23. Sautrot-Ba, P.; Jockusch, S.; Malval, J.-P.; Brezová, V.; Rivard, M.; Abbad-Andaloussi, S.; Blacha-Grzechnik, A.; Versace, D.-L. Quinizarin Derivatives as Photoinitiators for Free-Radical and Cationic Photopolymerizations in the Visible Spectral Range. *Macromolecules* **2020**, *53*, 1129–1141. [CrossRef]

24. Breloy, L.; Mhanna, R.; Malval, J.-P.; Brezová, V.; Jacquemin, D.; Pascal, S.; Siri, O.; Versace, D.-L. Azacalixphyrins as an innovative alternative for the free-radical photopolymerization under visible and NIR irradiation without the need of co-initiators. *Chem. Commun.* **2021**, *57*, 8973–8976. [CrossRef] [PubMed]

25. Iwamura, M.; Inamoto, N. Novel Formation of Nitroxide Radicals by Radical Addition to Nitrones. *Bull. Chem. Soc. Jpn.* **1967**, *40*, 703. [CrossRef]

26. Janzen, E.G.; Blackburn, B.J. Detection and identification of short-lived free radicals by an electron spin resonance trapping technique. *J. Am. Chem. Soc.* **1968**, *90*, 5909–5910. [CrossRef]

27. Chignell, C.F. Spin trapping studies of photochemical reactions. *Pure Appl. Chem.* **1990**, *62*, 301–305. [CrossRef]

28. Ouari, O.; Hardy, M.; Karoui, H.; Tordo, P. Recent developments and applications of the coupled EPR/Spin trapping technique (EPR/ST). In *Electron Paramagnetic Resonance*; The Royal Society of Chemistry: London, UK, 2010; Volume 22, pp. 1–40. [CrossRef]

29. Lauricella, R.; Allouch, A.; Roubaud, V.; Bouteiller, J.C.; Tuccio, B. A New Kinetic Approach to the Evaluation of Rate Constants for the Spin Trapping of Superoxide/Hydroperoxyl Radical by Nitrones in Aqueous Media. *Org. Biomol. Chem.* **2004**, *2*, 1304–1309. [CrossRef]

30. Criqui, A.; Lalevée, J.; Allonas, X.; Fouassier, J.-P. Electron Spin Resonance Spin Trapping Technique: Application to the Cleavage Process of Photoinitiators. *Macromol. Chem. Phys.* **2008**, *209*, 2223–2231. [CrossRef]

31. Janzen, E.G.; Stronks, H.J.; DuBose, C.M.; Poyer, J.L.; McCay, P.B. Chemistry and Biology of Spin-Trapping Radicals Associated with Halocarbon Metabolism in Vitro and in Vivo. *Environ. Health Perspect.* **1985**, *64*, 151. [CrossRef]

32. Lauricella, R.; Tuccio, B. Detection and Characterisation of Free Radicals After Spin Trapping. In *Electron Paramagnetic Resonance Spectroscopy: Applications*; Bertrand, P., Ed.; Springer International Publishing: Cham, Switzerland, 2020; pp. 51–82. [CrossRef]

33. Turro, N.J.; Khudyakov, I.V. Single-phase primary electron spin polarization transfer in spin-trapping reactions. *Chem. Phys. Lett.* **1992**, *193*, 546–552. [CrossRef]

34. Terabe, S.; Kuruma, K.; Konaka, R. ChemInform Abstract: Spin Trapping by Use of Nitroso-Compounds Part 6, Nitrosodurene And Other Nitrosobenzene Derivatives. *Chem. Inf.* **1973**, *4*, 1252–1258. [CrossRef]

35. Sautrot-Ba, P.; Brezová, V.; Malval, J.-P.; Chiappone, A.; Breloy, L.; Abbad-Andaloussi, S.; Versace, D.-L. Purpurin derivatives as visible-light photosensitizers for 3D printing and valuable biological applications. *Polym. Chem.* **2021**, *12*, 2627–2642. [CrossRef]

36. Sueishi, Y.; Nishihara, Y. Spin Trapping Chemistry of the Diphenylphosphinyl Radical. *J. Chem. Res.* **2001**, *2001*, 84–86. [CrossRef]

37. Chandra, H.; Davidson, I.M.T.; Symons, M.C.R. Unstable intermediates. Part 202. The use of spin traps to study trialkylsilyl and related radicals. *J. Chem. Soc. Perkin Trans.* **1982**, *2*, 1353–1356. [CrossRef]

38. Tuccio, B.; Zeghdaoui, A.; Finet, J.-P.; Cerri, V.; Tordo, P. Use of new β-phosphorylated nitrones for the spin trapping of free radicals. *Res. Chem. Intermed.* **1996**, *22*, 393–404. [CrossRef]

39. Lalevée, J.; Blanchard, N.; El-Roz, M.; Graff, B.; Allonas, X.; Fouassier, J.P. New Photoinitiators Based on the Silyl Radical Chemistry: Polymerization Ability, Esr Spin Trapping, and Laser Flash Photolysis Investigation. *Macromolecules* **2008**, *41*, 4180–4186. [CrossRef]

40. Versace, D.L.; Tehfe, M.A.; Lalevée, J.; Casarotto, V.; Blanchard, N.; Morlet-Savary, F.; Fouassier, J.P. Silyloxyamines as Sources of Silyl Radicals: Esr Spin-Trapping, Laser Flash Photolysis Investigation, and Photopolymerization Ability. *J. Phys. Org. Chem.* **2011**, *24*, 342–350. [CrossRef]

41. Telitel, S.; Vallet, A.-L.; Schweizer, S.; Delpech, B.; Blanchard, N.; Morlet-Savary, F.; Graff, B.; Curran, D.P.; Robert, M.; Lacôte, E.; et al. Formation of N-Heterocyclic Carbene–Boryl Radicals through Electrochemical and Photochemical Cleavage of the B–S bond in N-Heterocyclic Carbene–Boryl Sulfides. *J. Am. Chem. Soc.* **2013**, *135*, 16938–16947. [CrossRef]

42. Bouzrati-Zerelli, M.; Maier, M.; Dietlin, C.; Fabrice, M.-S.; Fouassier, J.P.; Klee, J.E.; Lalevée, J. A novel photoinitiating system producing germyl radicals for the polymerization of representative methacrylate resins: Camphorquinone/R 3 GeH/iodonium salt. *Dent. Mater.* **2016**, *32*, 1226–1234. [CrossRef]

43. Baumann, H.; Timpe, H.J.; Zubarev, V.E.; Fok, N.V.; Mel'nikov, M.Y. Lichtinitiierte Polymer- Und Polymerisations-Reaktionen Xxii: Untersuchungen Zur Photolyse Von Photo-Initiatoren Mit Benzyliden-Tert.-Butylamin-N-Oxid Als Spin-Trap. *J. Photochem.* **1985**, *30*, 487–500. [CrossRef]

44. Kura, H.; Oka, H.; Ohwa, M.; Matsumura, T.; Kimura, A.; Iwasaki, Y.; Ohno, T.; Matsumura, M.; Murai, H. Photochemistry and photocuring properties of thiol-substituted α-aminoalkylphenone as radical photoinitiator. *J. Polym. Sci. Part B Polym. Phys.* **2005**, *43*, 1684–1695. [CrossRef]

45. Teshima, W.; Nomura, Y.; Tanaka, N.; Urabe, H.; Okazaki, M.; Nahara, Y. ESR study of camphorquinone/amine photoinitiator systems using blue light-emitting diodes. *Biomaterials* **2003**, *24*, 2097–2103. [CrossRef]

46. Jockusch, S.; Landis, M.S.; Freiermuth, B.; Turro, N.J. Photochemistry and Photophysics of α-Hydroxy Ketones. *Macromolecules* **2001**, *34*, 1619–1626. [CrossRef]

47. Versace, D.-L.; Dubot, P.; Cenedese, P.; Lalevée, J.; Soppera, O.; Malval, J.-P.; Renard, E.; Langlois, V. Natural biopolymer surface of poly(3-hydroxybutyrate-co-3-hydroxyvalerate)-photoinduced modification with triarylsulfonium salts. *Green Chem.* **2012**, *14*, 788–798. [CrossRef]

48. Lalevée, J.; Poupart, R.; Bourgon, J.; Fouassier, J.-P.; Versace, D.-L. In situ production of visible light absorbing Ti-based nanoparticles in solution and in a photopolymerizable cationic matrix. *Chem. Commun.* **2015**, *51*, 5762–5765. [CrossRef]

49. Garra, P.; Brunel, D.; Noirbent, G.; Graff, B.; Morlet-Savary, F.; Dietlin, C.; Sidorkin, V.F.; Dumur, F.; Duché, D.; Gigmes, D.; et al. Ferrocene-based (photo)redox polymerization under long wavelengths. *Polym. Chem.* **2019**, *10*, 1431–1441. [CrossRef]

50. Lalevée, J.; Allonas, X.; Fouassier, J.; Tachi, H.; Izumitani, A.; Shirai, M.; Tsunooka, M. Investigation of the photochemical properties of an important class of photobase generators: The O-acyloximes. *J. Photochem. Photobiol. A Chem.* **2002**, *151*, 27–37. [CrossRef]

51. Chandra, H.; Davidson, I.M.T.; Symons, M.C.R. Use of spin traps in the study of silyl radicals in the gas phase. *J. Chem. Soc. Faraday Trans. 1 Phys. Chem. Condens. Phases* **1983**, *79*, 2705–2711. [CrossRef]

52. Detrembleur, C.; Versace, D.-L.; Piette, Y.; Hurtgen, M.; Jérôme, C.; Lalevée, J.; Debuigne, A. Synthetic and mechanistic inputs of photochemistry into the bis-acetylacetonatocobalt-mediated radical polymerization of n-butyl acrylate and vinyl acetate. *Polym. Chem.* **2011**, *3*, 1856–1866. [CrossRef]

53. El-Roz, M.; Lalevée, J.; Allonas, X.; Fouassier, J.P. Mechanistic Investigation of the Silane, Germane, and Stannane Behavior When Incorporated in Type I and Type II Photoinitiators of Polymerization in Aerated Media. *Macromolecules* **2009**, *42*, 8725–8732. [CrossRef]

54. Lalevée, J.; Peter, M.; Dumur, F.; Gigmes, D.; Blanchard, N.; Tehfe, M.-A.; Morlet-Savary, F.; Fouassier, J.P. Subtle Ligand Effects in Oxidative Photocatalysis with Iridium Complexes: Application to Photopolymerization. *Chem.—A Eur. J.* **2011**, *17*, 15027–15031. [CrossRef] [PubMed]

55. Tehfe, M.A.; Lalevée, J.; Allonas, X.; Fouassier, J.P. Long Wavelength Cationic Photopolymerization in Aerated Media: A Remarkable Titanocene/Tris(trimethylsilyl)silane/Onium Salt Photoinitiating System. *Macromolecules* **2009**, *42*, 8669–8674. [CrossRef]

56. Lalevée, J.; Blanchard, N.; Tehfe, M.-A.; Chany, A.-C.; Fouassier, J.-P. New Boryl Radicals Derived from N-Heteroaryl Boranes: Generation and Reactivity. *Chem.—A Eur. J.* **2010**, *16*, 12920–12927. [CrossRef]

57. Baban, J.A.; Marti, V.P.; Roberts, B.P. Ligated Boryl Radicals. Part 2. Electron Spin Resonance Studies of Trialkylamin–Boryl Radicals. *J. Chem. Soc. Perkin Trans.* **1985**, *2*, 1723–1733. [CrossRef]

58. Lacôte, E.; Curran, D.P.; Lalevée, J. NHC-Boranes: Air- and Water-tolerant Co-initiators for Type II Photopolymerizations. *CHIMIA* **2012**, *66*, 382–385. [CrossRef] [PubMed]

59. Jockusch, S.; Koptyug, I.V.; McGarry, P.F.; Sluggett, G.W.; Turro, N.J.; Watkins, D.M. A Steady-State and Picosecond Pump-Probe Investigation of the Photophysics of an Acyl and a Bis(acyl)phosphine Oxide. *J. Am. Chem. Soc.* **1997**, *119*, 11495–11501. [CrossRef]

60. Jockusch, S.; Turro, N.J. Phosphinoyl Radicals: Structure and Reactivity. A Laser Flash Photolysis and Time-Resolved ESR Investigation. *J. Am. Chem. Soc.* **1998**, *120*, 11773–11777. [CrossRef]

61. Sueishi, Y.; Miyake, Y. Spin Trapping of Phosphorus-Centered Radicals Produced by the Reactions of Dibenzoyl Peroxide with Organophosphorus Compounds. *Bull. Chem. Soc. Jpn.* **1997**, *70*, 397–403. [CrossRef]

62. Lalevée, J.; Morlet-Savary, F.; Tehfe, M.A.; Graff, B.; Fouassier, J.P. Photosensitized Formation of Phosphorus-Centered Radicals: Application to the Design of Photoinitiating Systems. *Macromolecules* **2012**, *45*, 5032–5039. [CrossRef]

63. Breloy, L.; Negrell, C.; Mora, A.-S.; Li, W.S.J.; Brezová, V.; Caillol, S.; Versace, D.-L. Vanillin derivative as performing type I photoinitiator. *Eur. Polym. J.* **2020**, *132*, 109727. [CrossRef]

64. Graceffa, P. Spin trapping the cysteine thiyl radical with phenyl-N-t-butylnitrone. *Biochim. Biophys. Acta (BBA)—Protein Struct. Mol. Enzym.* **1988**, *954*, 227–230. [CrossRef]

65. Ito, O.; Matsuda, M. Flash Photolysis Study for Substituent and Solvent Effects on Spin-Trapping Rates of Phenylthiyl Radicals with Nitrones. *Bull. Chem. Soc. Jpn.* **1984**, *57*, 1745–1749. [CrossRef]

66. Frejaville, C.; Karoui, H.; Culcasi, M.; Pietri, S.; Lauricella, R.; Tordo, P. 5-Diethoxyphosphoryl-5-methyl-1-pyrroline N-oxide (DEPMPO): A new phosphorylated nitrone for the efficient In Vitro and In Vivo spin trapping of oxygen-centred radicals. *J. Chem. Soc. Chem. Commun.* **1994**, *15*, 1793–1794. [CrossRef]

67. Frejaville, C.; Karoui, H.; Tuccio, B.; Le Moigne, F.; Culcasi, M.; Pietri, S.; Lauricella, R.; Tordo, P. 5-(Diethoxyphosphoryl)-5-methyl-1-pyrroline N-oxide: A New Efficient Phosphorylated Nitrone for the in Vitro and in Vivo Spin Trapping of Oxygen-Centered Radicals. *J. Med. Chem.* **1995**, *38*, 258–265. [CrossRef] [PubMed]

68. Breloy, L.; Brezová, V.; Blacha-Grzechnik, A.; Presset, M.; Yildirim, M.S.; Yilmaz, I.; Yagci, Y.; Versace, D.-L. Visible Light Anthraquinone Functional Phthalocyanine Photoinitiator for Free-Radical and Cationic Polymerizations. *Macromolecules* **2020**, *53*, 112–124. [CrossRef]

69. Breloy, L.; Losantos, R.; Sampedro, D.; Marazzi, M.; Malval, J.-P.; Heo, Y.; Akimoto, J.; Ito, Y.; Brezová, V.; Versace, D.-L. Allyl amino-thioxanthone derivatives as highly efficient visible light H-donors and co-polymerizable photoinitiators. *Polym. Chem.* **2020**, *11*, 4297–4312. [CrossRef]

70. Hoyle, C.E.; Bowman, C.N. Thiol–Ene Click Chemistry. *Angew. Chem. Int. Ed.* **2010**, *49*, 1540–1573. [CrossRef]

71. Hoyle, C.E.; Lee, T.Y.; Roper, T. Thiol-enes: Chemistry of the past with promise for the future. *J. Polym. Sci. Part A Polym. Chem.* **2004**, *42*, 5301–5338. [CrossRef]

72. Karlsson, H.; Lagercrantz, C.; Lemmich, J.; Torssell, K.; Shimizu, A. Spin Trapping of Some Phosphorus-centered Radical Species. *Acta Chem. Scand.* **1970**, *24*, 3411–3413. [CrossRef]

73. Abe, Y.; Seno, S.-Y.; Sakakibara, K.; Hirota, M. Spin trapping of oxygen-centred radicals by substituted N-benzylidene-tert-butylamine N-oxides. *J. Chem. Soc. Perkin Trans. 2* **1991**, *12*, 897–903. [CrossRef]

74. Murofushi, K.; Abe, K.; Hirota, M. Substituent effect on the spin-trapping reactions of substituted N-benzylidene-t-butylamine N-oxides. *J. Chem. Soc. Perkin Trans. 2* **1987**, *12*, 1829–1833. [CrossRef]

75. Dalal, D.P.; Eaton, S.S.; Eaton, G.R. The effects of lossy solvents on quantitative EPR studies. *J. Magn. Reson.* **1981**, *44*, 415–428. [CrossRef]

76. Buettner, G.R. Spin Trapping: ESR parameters of spin adducts 1474 1528V. *Free Radic. Biol. Med.* **1987**, *3*, 259–303. [CrossRef]

77. Leinisch, F.; Jiang, J.; DeRose, E.F.; Khramtsov, V.V.; Mason, R.P. Investigation of spin-trapping artifacts formed by the Forrester-Hepburn mechanism. *Free Radic. Biol. Med.* **2013**, *65*, 1497–1505. [CrossRef]

78. Buettner, G.R.; Kiminyo, K.P. Optimal EPR detection of weak nitroxide spin adduct and ascorbyl free radical signals. *J. Biochem. Biophys. Methods* **1992**, *24*, 147–151. [CrossRef]

79. Duling, D.R. Simulation of Multiple Isotropic Spin-Trap EPR Spectra. *J. Magn. Reson. Ser. B* **1994**, *104*, 105–110. [CrossRef]

80. Stoll, S.; Schweiger, A. EasySpin, a comprehensive software package for spectral simulation and analysis in EPR. *J. Magn. Reson.* **2006**, *178*, 42–55. [CrossRef]

81. Kotake, Y.; Kuwata, K. Electron Spin Resonance Study on the Difference of Structure in Diastereomeric Nitroxyl Radicals. *Bull. Chem. Soc. Jpn.* **1981**, *54*, 394–398. [CrossRef]

82. Finkelstein, E.; Rosen, G.M.; Rauckman, E.J. Spin Trapping of Superoxide and Hydroxyl Radical: Practical Aspects. *Arch. Biochem. Biophys.* **1980**, *200*, 1–16. [CrossRef]

83. Ranguelova, K.; Mason, R.P. The fidelity of spin trapping with DMPO in biological systems. *Org. Magn. Reson.* **2011**, *49*, 152–158. [CrossRef]

84. Rosen, G.M.; Rauckman, E.J. Spin trapping of the primary radical involved in the activation of the carcinogen N-hydroxy-2-acetylaminofluorene by cumene hydroperoxide-hematin. *Mol. Pharmacol.* **1980**, *17*, 233–238. [PubMed]

85. Chandra, H.; Symons, M.C.R. Hydration of spin-trap cations as a source of hydroxyl adducts. *J. Chem. Soc. Chem. Commun.* **1986**, *16*, 1301–1302. [CrossRef]

86. Eberson, L. Inverted Spin Trapping'. Reactions between the Radical Cation of A-Phenyl-N-Tert-Butylnitrone and Ionic and Neutral Nucleophiles. *J. Chem. Soc. Perkin Trans.* **1992**, *2*, 1807–1813. [CrossRef]

87. Zubarev, V.; Brede, O. Direct detection of the cation radical of the spin trap α-phenyl-N-tert-butylnitrone. *J. Chem. Soc. Perkin Trans.* **1994**, *2*, 1821–1828. [CrossRef]

88. Forrester, A.R.; Hepburn, S.P. Spin Traps. A Cautionary Note. *J. Chem. Soc. C* **1971**, 701–703. [CrossRef]

89. Eberson, L. Inverted Spin Trapping. Part Iii. Further Studies on the Chemical and Photochemical Oxidation of Spin Traps in the Presence of Nucleophiles. *J. Chem. Soc. Perkin Trans.* **1994**, *2*, 171–176. [CrossRef]

90. Tuccio, B.; Lauricella, R.; Fréjaville, C.; Bouteiller, J.-C.; Tordo, P. Decay of the hydroperoxyl spin adduct of 5-diethoxyphosphoryl-5-methyl-1-pyrroline N-oxide: An EPR kinetic study. *J. Chem. Soc. Perkin Trans.* **1995**, *2*, 295–298. [CrossRef]

91. Potapenko, D.I.; Bagryanskaya, E.G.; Tsentalovich, Y.P.; Reznikov, V.A.; Clanton, T.L.; Khramtsov, V.V. Reversible Reactions of Thiols and Thiyl Radicals with Nitrone Spin Traps. *J. Phys. Chem. B* **2004**, *108*, 9315–9324. [CrossRef]